Defect production in collision cascades in elemental semiconductors and fcc metals

K. Nordlund
Materials Research Laboratory, University of Illinois, Urbana, Illinois 61801
and Accelerator Laboratory, P.O. Box 43, FIN-00014 University of Helsinki, Finland

M. Ghaly and R. S. Averback
Materials Research Laboratory, University of Illinois, Urbana, Illinois 61801

M. Caturla and T. Diaz de la Rubia
Lawrence Livermore National Laboratory, Livermore, California 94550

J. Tarus
Accelerator Laboratory, P.O. Box 43, FIN-00014 University of Helsinki, Finland
(Received 14 October 1997)

A comparative molecular dynamics simulation study of collision cascades in two elemental semiconductors and five fcc metals is performed to elucidate how different material characteristics affect primary defect production during ion irradiation. By using simulations of full 400 eV-10 keV collision cascades and contrasting the results on different materials with each other, we probe the effect of the mass, melting temperature, material strength, and crystal structure on the modification of the material due to the cascade. The results show that the crystal structure has a strong effect on many aspects of damage production, while other material characteristics are of lesser overall importance. In all materials studied, isolated point defects produced by the cascade are predominantly interstitials. In semiconductors, amorphous clusters are produced in the cascade core, whereas in metals most of the crystal regenerates, leaving only small vacancy-rich clusters. Large interstitial clusters found in a few events in the heavy metals were observed to form by the isolation of a high-density liquid zone during the recrystallization phase of a cascade. [S0163-1829(98)01813-X]

I. INTRODUCTION

The nature of damage produced in solids during ion irradiation is a long-standing problem of considerable practical interest. While the overall picture of the time evolution of collision cascades is now becoming clear,[1] many important details are understood in only very imprecise terms. Until these details are clarified, the goal of predicting the evolution of damage in materials used in such technologies as ion implantation, beam-assisted deposition, and nuclear power generation will remain largely unrealized.

One of the reasons why cascade dynamics is not very well understood is the near impossibility to experimentally study the very rapid processes occurring inside materials during ion irradiation. Analyzing femtosecond-scale lifetimes of excited nuclei does provide a means to probe the initial development of a cascade,[2] but the method is not sensitive to the thermal spike phase of the cascade and hence useful primarily for making comparisons between different repulsive potentials.[3] Experimental studies of sputtering,[4] surface damage,[5] mixing,[6] and final damage structures,[7] on the other hand, primarily probe the end result of the cascade.

Different computer simulation methods have been widely employed to bridge the gap between the known experimental initial irradiation conditions, such as the beam energy and sample structure, and the measurable end results. Deterministic molecular dynamics (MD) simulation methods provide a good way to study the initial development of the cascade, including the ballistic collision phase, the thermal spike phase, and even the fast defect migration processes occurring in the immediate vicinity of the heat spike[8,9] on time scales of the order of a few nanoseconds. Kinetic Monte Carlo studies, moreover, have been used to study the damage evolution after the heat spike over time scales of the order of thousands of seconds.[10] Although a fairly coherent picture of the overall nature of the final damage in the cascades is emerging at least in some materials,[11–13] the reasons why semiconductors and metals appear to behave quite differently are still not understood.

The first step in attempting to understand the mechanisms of damage production is to study damage production at low ($T \lesssim 100$ K) temperatures, where damage migration and annealing processes do not complicate the picture. This regime is ideally suited for study by molecular dynamics simulations. Many such simulations have now been performed on metals, although primarily in $3d$ transition metals and ordered alloys.[14–19] Simulations of high-energy cascades in semiconductors have been performed mostly in Si.[13,20,21] These studies, moreover, have been concerned mostly with defect production and have neglected other quantities such as ion beam mixing. As a consequence systematic investigations of cascades in metals and semiconductors are still needed to answer why each material responds to particle radiation as it does.

In the present paper we perform a comparative study of seven different materials to examine the damage production mechanisms in a relatively wide range of materials and recoil energies. Included in the study are the semiconductors Si and

TABLE I. Some properties of the materials treated in the present study. Z is the atomic number, m the mass, ρ_{at} the atomic density, T_{melt} the melting temperature, and B the bulk modulus. V_{at}/V_{lat} is the volume of the largest possible atom sphere not overlapping other atoms, divided by the volume per atom in the lattice, $V_{lat}=1/\rho_{at}$, and is thus a measure of how close packed the lattice is. The values for T_{melt} and B are those calculated by the interatomic potentials, both of which were determined by MD simulations as part of the present study.

Element	Z	m (amu)	ρ_{at} (atoms/Å^3)	V_{at}/V_{lat}	T_{melt} (K)	B (GPa)
Si[a]	14	28.1	0.050	0.34	1700	101
Si[b]	14	28.1	0.050	0.34	2400	98
Ge[a]	32	72.6	0.044	0.34	2900	80
Ge[c]	32	72.6	0.044	0.34	1230	66
Al	13	27.0	0.060	0.74	940	81
Ni	28	58.7	0.092	0.74	1700	180
Cu[d]	29	63.5	0.085	0.74	1290	138
Cu[e]	29	63.5	0.085	0.74	1280	142
Pt[d]	78	195.1	0.066	0.74	1530	283
Pt[f]	78	195.1	0.066	0.74	2130	283
Au	79	197.0	0.059	0.74	1110	167

[a]Stillinger-Weber potential (Ref. 33).
[b]Tersoff potential (Ref. 36).
[c]Ge potential with T_{melt} correction (see text).
[d]Unmodified Foiles potential (Ref. 29).
[e]Sabochick-Lam potential (Ref. 30).
[f]Pt potential with T_{melt} correction (see text).

Ge and the fcc metals Al, Ni, Cu, Pt, and Au. Although cascades in Si (Refs. 13 and 21) and Cu (Refs. 22 and 23) have been studied carefully previously, we include them in the present study so that we can compare the different materials under the same conditions of energy and target temperature, and ensure that the quantities we use for the comparison are evaluated the same way in all materials. Furthermore, two different interatomic potentials were used to study these two elements, and also Ge and Pt, to obtain a picture of the reliability of the models used.

Since Al and Si have nearly the same mass, and differ by only 20% in atomic density (see Table I), comparison of cascades in them elucidates the effects of crystal structure on damage production. Comparison of the results in these light elements to those in the heavier elements probes the effect of the atom mass on the outcome of the cascades, and contrasting results in the relatively soft materials (with low melting points) Cu and Au to the harder materials Ni and Pt probes the effect of the material hardness and melting point on the results.

This paper is organized as follows. In the next section we present our simulation methods and the interatomic potentials used. In Sec. III we discuss damage production in semiconductors and in Sec. IV we present the metal results and compare the metals to the semiconductors.

II. SIMULATION PRINCIPLES

Classical molecular dynamics simulations were used to simulate collision cascades. Periodic boundary conditions were applied to the fixed-size simulation cells, which contained 25–40 atoms for every electron volt of recoil energy of the initial recoil.

The temperature of the cell was initialized to 0 K and scaled softly down towards zero at the outermost three atomic layers during the cascade event. The scaling was fine-tuned to prevent reflection and transmission of the pressure wave emanating from the cascade. Although using a ambient temperature of 0 K is of course *per se* unrealistic, earlier simulation studies have shown that except possibly for the length of replacement collision sequences (RCS's) in metals, damage production at temperatures below 100 K does not significantly depend on the temperature. On the other hand, using a cell temperature of 0 K simplifies the task of distinguishing which damage production effects are directly caused by the cascade itself. Since we are in the present study interested in the fundamental mechanisms of damage production rather than any specific practical application, the choice of 0 K as the ambient temperature seemed appropriate.

A variable time step,[24] linkcell method,[25] and two-dimensional spatial decomposition of the simulation cell for message-passing parallel computers were employed to speed up the simulations.

The forces acting between the atoms were described with semiempirical many-body potentials. The melting points and bulk moduli of all the potentials are given in Table I. The melting points were determined in the present study by simulating a liquid-solid interface at different temperatures until an equilibrium temperature was found.[26]

For the metals we employed embedded-atom method (EAM) potentials, which have been found to describe a broad spectrum of atomistic-level properties relatively well, and are well motivated theoretically.[27] For Al we used the potential by Ercolessi and Adams[28] and for Ni, Cu,

Pt, and Au the original EAM potentials formulated by Foiles.[29] For Cu we also used the potential by Sabochick and Lam.[30]

The original Pt EAM potential underestimates the melting point by more than 500 K. Therefore, we also used a modified Pt potential which was constructed to reproduce the experimental melting point and threshold displacement energy to an accuracy of a few percent (the unmodified potential had a somewhat too low minimum threshold displacement energy). The modification was done by strengthening the potential for separations smaller than the nearest-neighbor distance, which ensured that the close-to-equilibrium properties modeled well by the unmodified potential were not affected by the modification. We also checked that the interstitial formation energy and volume were still reasonable after the modification.

A large number of interatomic potentials have been proposed for describing tetrahedral semiconductors. None of them, however, appears to have the wide range of applicability of the EAM potentials.[31] The wide use of ion implantation methods in the semiconductor industry, however, adds importance to knowing the nature of the damage produced in Si. In previous molecular dynamics simulation studies[13,23,32] most authors have employed the well-tested Stillinger-Weber interatomic potential to describe Si.[33] This potential is well suited for describing irradiation studies primarily because it describes both liquid and solid properties fairly well, and does give the correct ordering of point defects with respect to their formation energies.[34] Unless otherwise mentioned, the Si results discussed in this study derive from the Stillinger-Weber potential. It has been argued that this potential penalizes bonding types other than the ideal tetrahedral bonding too strongly,[35] however. This might lead to an unrealistically strong regeneration of the distorted liquid and amorphous zones resulting from a cascade. The Tersoff interatomic potential,[36] on the other hand, describes most Si bonding types quite well, and has many other attractive features,[31] even though it does not give the right ordering of point defect energies. Since the formulations and properties of the Tersoff and Stillinger-Weber potentials are quite different, comparing cascade results obtained by each potential offers a way to estimate to what extent the simulation results in Si may be artifacts of the classical potentials. To this end, we performed a systematic study of 400 eV–5 keV cascades with both potentials.

For Ge we used the Stillinger-Weber-type potential from Ref. 37. We found, however, that this potential gave a melting point of 2900 K, which is more than twice the experimental value of 1211 K. The Stillinger-Weber potential for Si uses a slightly reduced cohesive energy to reproduce the experimental melting point.[33] Since previous simulations on metals suggest that a realistic melting point is important for cascade calculations, we modified the cohesive energy of the Ge potential to reproduce the experimental melting point.

Using the potential parameters $\lambda = 21$ (as in Ref. 38) and an 18%-reduced cohesive energy $\varepsilon = 1.58$ eV, we obtained 1230 ± 50 K for the melting point of the modified potential. The bulk modulus was also reduced by 18% due to this modification, which we think is acceptable considering that other semiconductor potentials have comparable errors in their values for the elastic moduli.[31] It is encouraging that the threshold displacement energy of the modified potential was reduced from 25 eV to 13 eV, which is in good agreement with the experimental value of 15 eV.[39] Also, we found recently that mixing results obtained with the modified potential are close to experimental values,[40] whence we will use the results of the modified potential as our primary Ge results. As a measure of the sensitivity of damage results to the potential, we simulated 400 eV–5 keV cascades with both Ge potentials.

All of the many-body potentials were smoothly joined to a repulsive potential that describes well the energetic short-range interactions; for Si and Ge we used potentials obtained from *ab initio* calculations,[40] and for the metals the Ziegler-Biersack-Littmark (ZBL) interatomic potential.[41] Even though the ZBL potential is not particularly accurate,[40] in metals most end results of the cascade are a result of the behavior of the liquid zone, which is not affected by the choice of the repulsive potential. Also, studies of low-energy cascades in Si have shown that defect production even in semiconductors is not sensitive to small errors in the repulsive potential.[42] The joining of the repulsive potential governing high-energy collisions to the low-energy part was calibrated so that the joined potential reproduced experimental displacement energies[39,43] well. With the exception of the unmodified Pt and Ge potentials discussed above and the Sabochick-Lam potential discussed in Sec. IV C 2, the joined potentials reproduced the experimental threshold displacement energies well, with errors of 0–20 %. The Ni, Cu, and Pt potentials were also compared with experimental high-pressure equations of state.[44,45] The potentials were found to be in good agreement with the experimental data in the pressure regime below 100 GPa relevant in collision cascades.[11]

The collision cascades were initiated by giving one of the atoms in the lattice a recoil energy of 400 eV–10 keV. The initial velocity direction of the recoil atom was chosen randomly. To obtain representative statistics, 5–14 events were simulated for each energy and material. The evolution of each cascade was followed for 20–30 ps.

The electronic stopping power was included in the runs as a nonlocal frictional force affecting all atoms with a kinetic energy higher than 10 eV. For Si we used an experimental stopping power[46] and for the other elements SRIM96 stopping powers.[41,47] We did not include a model of the electron-phonon coupling for the metals. It is unclear how it should be treated. Conventionally it is believed to affect damage production in Ni and Pt, but to be relatively unimportant in Cu and Au.[14,48] Our recent comparison of ion beam mixing simulations and experiments suggests that the coupling may in fact be significantly less important than has been suggested.[49] The coupling was excluded both because of the large uncertainties about how it should be treated, and because its inclusion would have obscured our attempt to deduce the effect of basic materials characteristics on damage production.

The mixing parameter was calculated in the simulations using the expression

$$Q = \frac{[r_i(t) - r_i(t=0)]^2}{6 n_0 E_{D_n}}, \tag{1}$$

where n_0 is the atomic density and E_{D_n} the deposited nuclear energy. E_{D_n} was obtained from the difference of the initial recoil energy and the total energy lost to electronic slowing down.

During the simulations, an atom was labeled ''liquid'' or ''hot'' if the the average kinetic energy of it and its nearest neighbors was above an energy corresponding to the melting point of the material through the usual relation between temperature and kinetic energy, $E=\frac{3}{2}kT$. This designation is useful for illustrating which part of a simulation cell has been affected by a cascade. In a previous study we found that the kinetic energy criterion provided a good approximation to a more sophisticated structure factor method.[9]

Examination of the cascades shows that the number of energetic atoms in all materials has a very strong peak during the first 0.1–0.5 ps. Since this is a direct result of the thermalization of the ballistic recoils formed initially, these ''liquid'' atoms do not correspond to the classical concept of a liquid in any meaningful way. After this transient phase, however, one or a few continuous regions of hot atoms may form and exist for 5–20 ps. Although the quench rate of such ''liquid pockets'' is enormous, these regions have been found to correspond to a classical liquid in the sense that atoms move around each other freely and the pair distribution function resembles that of a liquid in equilibrium.[50,51] Since it is known that local equilibration requires only ~ 3 collisions of hard spheres, we call the energetic atoms which have experienced less than than 3–5 lattice vibrations ''hot'' and the others ''liquid.''

Interstitials and vacancies were recognized in the simulations using a Wigner-Seitz cell analysis of the atom positions with respect to the lattice defined by undisturbed simulation cell regions.[52] A lattice site with an empty Wigner-Seitz cell was labeled a vacancy and a cell with multiple atoms an interstitial. The applicability of this method to semiconductors is discussed in Sec. III A 1.

The relationship between the ion range and the distribution of final damage was examined by calculating the mean chord range of recoils starting from a lattice site using the MDRANGE method.[24,49]

The results from the simulations are summarized in Table II. The table lists the initial energy E; the deposited nuclear energy E_{D_n}; the average number number of interstitials remaining after the cascade, N_{int}; the mixing Q; the number of atoms displaced by more than half the nearest-neighbor distance, N_{displ}; the maximum number of hot atoms, $N_{\mathrm{hot,max}}$; the root-mean-square (rms) distance $\langle dR_{\mathrm{int}}\rangle$ of interstitials away from the interstitial center of mass; and the mean chord range $\overline{R}$ of primary recoils (since $\overline{R}$ is calculated using MDRANGE it is independent of the choice of the potential). The number of defects, N_{int}, given is the number of Wigner-Seitz interstitial sites. All the values given in the table are averages over several events. The uncertainties in the table are the errors of the average $\sigma_{\overline{x}}=\sigma/\sqrt{N}$; since the number of events simulated was in most cases 6–8, the standard deviation σ of the results is roughly 3 times the error.

III. SEMICONDUCTORS

A. Silicon

The understanding of the initial states of damage produced by irradiation of Si relies mainly on computer simulations, as the available experimental methods give little direct and unambiguous information about small-scale defects in Si. Classical MD methods have recently given a consistent overall picture of damage production in cascades.

The primary findings of these past studies can be summarized as follows. Replacement collision sequences, which are quite important in metals, have been shown to be very short in Si due to the lack of close-packed directions in the diamond crystal structure.[53] Collision cascades at an energy of 5 keV have been shown to be completely broken down into subcascades[54] in the form of small, isolated liquidlike pockets.[21] When these zones cool down, they form amorphouslike damage pockets. At high temperatures these pockets anneal out rapidly,[13] but at room temperature and below at least the largest amorphous pockets are stable, and have been observed experimentally.[55] Defects outside the damage zones tend to be predominantly interstitials.[13] The previous MD cascade studies have used either the Tersoff[9,20] or the Stillinger-Weber interatomic potential,[13,21,53,56] but no study has done a one-to-one comparison of cascade results obtained with the two potentials even though there are indications that damage production in Si cascades can vary strongly even with small differences in the interatomic potential.[42]

The present study complements the previous work in silicon by studying self-cascades in a wide energy range and comparing two different interatomic potentials directly. While some of the qualitative results obtained with the Stillinger-Weber potential will be similar to those found in previous studies, these results provide a basis for the comparison with the Si Tersoff potential results and with the Al and Ge results.

1. Damage analysis methods in Si

The damage produced by high-energy cascades in covalently bonded materials tends to be of a complex nature. Hence even the question of how one should analyze the final damage state has no obvious answer. Various authors have employed different criteria for recognizing defects: potential energy,[57] analysis of atomic bonding,[58] small Lindemann spheres centered on lattice sites,[59] spheres with the size of half a nearest-neighbor distance,[13] and Wigner-Seitz cells.[60] To clarify how damage results obtained by different means relate to one another, we first recall and compare them here. In the remainder of this discussion, the Si results are primarily presented in terms of Wigner-Seitz cell defects[52] to make them easily comparable to results in metals.

The perhaps simplest way of recognizing damaged regions at low temperatures is to label all atoms with a potential energy significantly (typically, 0.2 eV) higher than the equilibrium value disordered. This is a convenient way of indicating which parts of a simulation cell contain damage and studying large defects like dislocations,[57] but it does not give a detailed picture of the defect structures on an atomic level.

Three commonly used geometric methods of recognizing defects consist of using Lindemann spheres, nearest-neighbor spheres, or Wigner-Seitz cells. In these methods, the atom positions in a simulation cell are analyzed with respect to a geometric structure centered on ideal lattice sites defined by the undisturbed lattice surrounding the damaged

TABLE II. Average values and standard deviations for the results of the cascades. Each figure is an average over at least four different events. The notation is explained in the text.

Element	E (keV)	E_{D_n} (keV)	N_{int}	Q (Å^5/eV)	N_{displ}	$N_{\text{hot,max}}$	$\langle dR_{\text{int}} \rangle$ (Å)	$\overline{R}$ (Å)
Si[a]	0.4	0.35	4.1 ± 0.5	6.0 ± 0.5	27 ± 2	132 ± 3	11.6 ± 0.3	21 ± 1
	2.0	1.6	17 ± 1	10 ± 1	120 ± 4	710 ± 30	23.8 ± 0.8	56 ± 2
	5.0	3.8	43 ± 1	13 ± 1	340 ± 10	1350 ± 30	41 ± 1	102 ± 4
	10.0	7.5	97 ± 5	16 ± 1	700 ± 50	3100 ± 100	56 ± 2	190 ± 10
Si[b]	0.4	0.35	8.3 ± 0.2	5.9 ± 0.2	25 ± 1	–	12.7 ± 0.2	21 ± 1
	2.0	1.6	39 ± 2	11 ± 1	128 ± 4	–	24.4 ± 0.6	56 ± 2
	5.0	3.9	84 ± 2	11 ± 1	300 ± 10	–	36 ± 1	102 ± 4
Ge	0.4	0.34	4.6 ± 0.3	9.7 ± 0.3	46 ± 2	300 ± 100	13.6 ± 0.6	13 ± 1
	2.0	1.6	47 ± 2	16 ± 0.5	330 ± 10	1200 ± 100	18.5 ± 0.5	34 ± 1
	5.0	3.8	141 ± 5	26 ± 1	1100 ± 30	2600 ± 100	25.0 ± 0.5	56 ± 2
	10.0	7.6	340 ± 30	30 ± 3	2300 ± 200	5500 ± 500	35 ± 1	85 ± 4
Ge[c]	0.4	0.35	2.4 ± 0.1	5.1 ± 0.4	17 ± 1	150 ± 5	5.5 ± 0.6	13 ± 1
	2.0	1.6	12 ± 1	7.8 ± 0.3	88 ± 4	600 ± 100	25 ± 1	34 ± 2
	5.0	3.9	27 ± 1	10.4 ± 0.4	210 ± 10	1200 ± 200	38 ± 1	56 ± 2
Al	0.4	0.35	2.0 ± 0.2	4.1 ± 0.2	80 ± 5	200 ± 20	8.5 ± 0.9	15 ± 1
	2.0	1.6	13 ± 1	9 ± 1	230 ± 20	1450 ± 60	25 ± 2	50 ± 2
	10.0	7.7	48 ± 3	10 ± 1	900 ± 100	6000 ± 1000	62 ± 2	190 ± 10
Ni	0.4	0.34	2.0 ± 0.1	1.1 ± 0.1	20 ± 1	60 ± 3	9 ± 1	6 ± 1
	2.0	1.6	4.8 ± 0.4	2.1 ± 0.1	170 ± 7	830 ± 30	18 ± 1	14 ± 1
	10.0	7.8	16 ± 1	4.3 ± 0.2	1400 ± 40	5000 ± 200	35 ± 2	43 ± 2
Cu[d]	0.4	0.35	1.8 ± 0.2	2.0 ± 0.1	28 ± 2	86 ± 4	7.3 ± 0.5	6 ± 1
	2.0	1.6	6.4 ± 0.4	4.7 ± 0.2	370 ± 10	1250 ± 40	18.4 ± 0.7	15 ± 1
	10.0	7.9	15 ± 2	13 ± 1	3000 ± 10	7000 ± 400	35 ± 2	47 ± 2
Cu[e]	0.4	0.34	1.8 ± 0.2	1.2 ± 0.1	22 ± 2	170 ± 10	4.1 ± 0.8	6 ± 1
	2.0	1.6	6.0 ± 0.5	3.2 ± 0.2	220 ± 10	1300 ± 50	18.7 ± 0.5	15 ± 1
	10.0	8.0	16 ± 2	9.5 ± 0.5	2600 ± 50	7100 ± 400	33 ± 2	47 ± 2
Pt	0.4	0.33	1.3 ± 0.1	1.3 ± 0.1	17 ± 1	91 ± 4	1 ± 1	5 ± 1
	2.0	1.6	3.1 ± 0.3	2.3 ± 0.1	122 ± 3	670 ± 20	17 ± 2	11 ± 1
	10.0	7.6	7 ± 1	6.1 ± 0.2	1050 ± 30	4300 ± 100	41 ± 1	32 ± 2
Pt[f]	0.4	0.32	1.9 ± 0.1	3.6 ± 0.2	39 ± 3	77 ± 5	10 ± 1	5 ± 1
	2.0	1.5	4.6 ± 0.2	7.0 ± 0.3	300 ± 10	830 ± 30	23 ± 1	11 ± 1
	10.0	7.3	9 ± 2	22 ± 1	2330 ± 20	6000 ± 200	31 ± 1	32 ± 2
Au	0.4	0.32	1.3 ± 0.1	4.3 ± 0.1	42 ± 1	170 ± 10	5 ± 1	5 ± 1
	2.0	1.5	3.7 ± 0.2	12.6 ± 0.6	400 ± 10	1250 ± 70	19 ± 2	12 ± 1
	10.0	7.0	15 ± 3	60 ± 2	3350 ± 50	6700 ± 200	31 ± 3	32 ± 2

[a]Stillinger-Weber potential (Ref. 33).
[b]Tersoff potential (Ref. 36).
[c]Unmodified Ge potential with a too high melting point (see text).
[d]Foiles potential (Ref. 29).
[e]Sabochick-Lam potential (Ref. 30).
[f]Unmodified Pt potential with a too low melting point (see text).

regions. If the geometric structure contains no atoms, the lattice position is labeled a vacancy. The structure can be either a sphere with the Lindemann radius r_{L} (0.45 Å for Stillinger-Weber Si), a sphere with a radius equal to half the nearest-neighbor distance r_{NN}, or a Wigner-Seitz-cell–Voronoy polyhedron[52] centered on a lattice site. The motivation behind using the Lindemann sphere criterion, and how to recognize disordered atom regions using it, has been dis-

TABLE III. Number of defects in a few individual 5 keV cascades and an amorphous damage sphere in Si analyzed with different methods. V_{WS} indicates the number of vacancies obtained using a Wigner-Seitz-cell–Voronoy-polyhedron analysis, V_L vacancies recognized using Lindemann spheres, and V_{NN} vacancies obtained using nearest-neighbor spheres. N_p gives the number of atoms with a potential energy at least 0.2 eV above the equilibrium value.

Damage label	V_{WS}	V_L	V_{NN}	N_p
5kev12	35	283	104	404
5kev13	44	355	116	367
5kev14	54	433	139	546
5kev15	50	386	121	497
Amorph.	30	219	99	200

cussed recently by Hensel and Urbassek.[59] The Wigner-Seitz cell analysis has the advantage that it is space filling, and does not involve an arbitrary cutoff size.

The difference in the amount of damage obtained using the different criteria described above was found by analyzing a few (Stillinger-Weber potential) 5 keV events using all methods. In addition, the methods were also used to analyze the defect state of an amorphous pocket of radius $2a_0$ embedded in an undamaged Si crystal. The results shown in Table III give the number of vacancies obtained with the geometric criteria and the number of disturbed atoms evaluated with the potential energy criterion.

The results in the table show that for damage from keV cascades in Si, the amount of damage obtained with different criteria varies greatly, which is not surprising considering their strongly differing definitions. But the values for any given event have roughly the same ratios in all cases,

$$V_L \approx 8 V_{WS},$$
$$V_{NN} \approx (2.5-3.0) V_{WS}, \quad (2)$$
$$N_p \approx (8-11) V_{WS},$$

which indicates that the methods can be expected to give fairly consistent trends. The last relation gives the useful rule of thumb for Si that the total number of disordered atoms is roughly 10 times the number of Wigner-Seitz vacancies or interstitials. It is interesting to note that these same relations are fairly well obeyed by the artificial amorphous sphere as well. Note, however, that in the amorphous zone the vacancy concentration is over 100% using the Lindemann sphere criterion, indicating that it can be quite misleading for large-scale damage. In fact this brief study illustrates that none of these definitions is truly satisfactory in describing the defect state of an amorphous pockets primarily because defects in amorphous pockets are not amenable to these descriptions. But the Wigner-Seitz method applied on amorphous zones does have the advantage that it immediately tells whether the pocket has an excess or deficiency of atoms compared to an undisturbed lattice. The nature of this damage will be examined more closely in Sec. III A 3 below.

2. Difference between Tersoff and Stillinger-Weber Si

The values in Table II show that the results in silicon modeled by the Tersoff potential are almost the same within the uncertainties as those in silicon modeled by the Stillinger-Weber potential, with the exception of the final number of defects. Since heat spikes are very short-lived in silicon, quantities like ion beam mixing and number of displaced atoms will be mostly affected by the crystal structure and the repulsive part of the potential. These are the same for both potentials, and so it is not surprising that the results are about the same. The final number of defects, on the other hand, is about a factor of 2 larger for the Tersoff potential. The time evolution of the number of Wigner-Seitz defects for one representative event simulated with each potential is illustrated in Fig. 1. The initial development of the number of defects is similar for both potentials. This is to be expected, since both potentials have the same repulsive part, which determines the outcome of the ballistic part of the simulation. As the cascades cool down and the relevance of the repulsive part of the potentials lessens, the differences in the two potentials come more into play.

The Tersoff potential simulation reaches a stable defect value in about 1 ps, whereas the defect value obtained with the Stillinger-Weber potential continues to decrease for a few picoseconds after the initiation of the cascade. Because the Tersoff potential gives relatively low energies for under- and overcoordinated bonding configurations,[35] it allows the complex damage formed in the ballistic phase of the cascade to freeze in with very little regeneration of the lattice, resulting in a larger amount of final damage in the lattice. The Stillinger-Weber potential, on the other hand, is fitted only to the tetrahedral configuration and penalizes nontetrahedral bonding types. Therefore, this potential favors regeneration

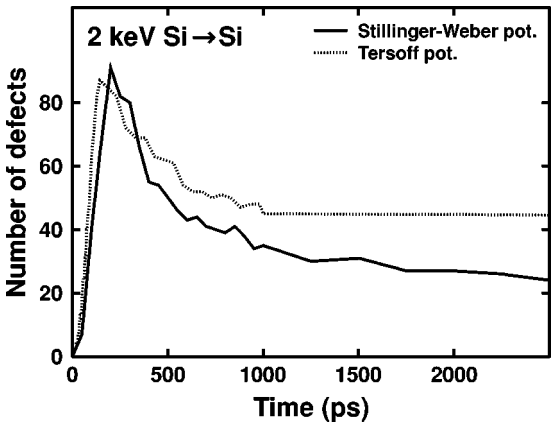

FIG. 1. Number of defects as a function of time in two representative 2 keV cascades simulated using the Tersoff and Stillinger-Weber interatomic potentials.

of damage into an ideal diamond lattice structure, explaining why the damage level decreases further than for the Tersoff potential. The lower melting point of the Stillinger-Weber potential, moreover, allows more time for regeneration before the defect structure freezes in. The difference in the amount of damage is significant, about a factor of 2.

Analysis of the distribution of defects in clusters (using the r_{cl} analysis described below) showed that the number of isolated point defects is about the same for the two potentials. This is a consequence of most isolated defects being formed by energetic recoils, whose behavior is dominated by the pair potential. But the number of defects in clusters is clearly larger for the Tersoff than the Stillinger-Weber potential. The larger number of defects of the Tersoff potential is thus located in damage clusters, as expected from the argument above.

The potential comparison indicates that classical potentials give a fairly reliable picture of the production of isolated point defects. Since experimental data on damage production in silicon are difficult to translate into the actual number of defects or their structure (see, e.g., Ref. 62), there is presently no means to determine which of the two potentials gives a more realistic picture of the the amorphous damage pockets. In the near future, it may be possible to calculate low-energy cascades with physically more realistic tight-binding MD methods[58,63] to clarify the situation.

3. Final state of damage

As expected from previous studies,[21] the 10 keV cascades in Si are clearly broken up into spatially separated subcascades (see Fig. 2). Animations of 400 eV and 2 eV cascades showed that the former were not broken down into subcascades, while the latter were, indicating that the threshold for subcascade formation in Si is only about 1 keV. Figure 3 shows, moreover, that the final damage is located in the same cell regions that were hot during the development of the cascade, but clearly the damage volume is smaller than in Fig. 2. It is also apparent that some of the hot atoms in the figure are still on lattice sites. Additionally some damage annealing does occur during the cascade for the Stillinger-Weber potential. As noted above, a similar recombination is largely absent in the Tersoff potential simulations. Many of the interstitials in Fig. 3 (indicated by circles) appear to be located outside the center of the amorphous zones.

Table II shows that the number of final defects, N_{int}, and the number of displaced atoms, N_{displ}, in the cascades in silicon increases linearly with the deposited nuclear energy E_{D_n}, which can be expected since the cascades are in the subcascade regime.

We made a detailed analysis of the nature of the final damage produced by the Si, Ge, and Al cascades. All (Wigner-Seitz) defects which were within a certain radius r_{cl} of any other defect were interpreted to be adjacent. All defects within the same network of adjacent defects were interpreted to form one cluster. The results of this analysis are somewhat arbitrary, as they will depend on the choice of r_{cl}. But a reasonable choice of the value for r_{cl} in Si is between a_0 and 2 a_0. Values less than a_0 could lead to amorphous zones not being recognized as continuous. Recent diffuse scattering experimental results, on the other hand, indicate that Frenkel pairs in Si separated by roughly 1 nm are stable

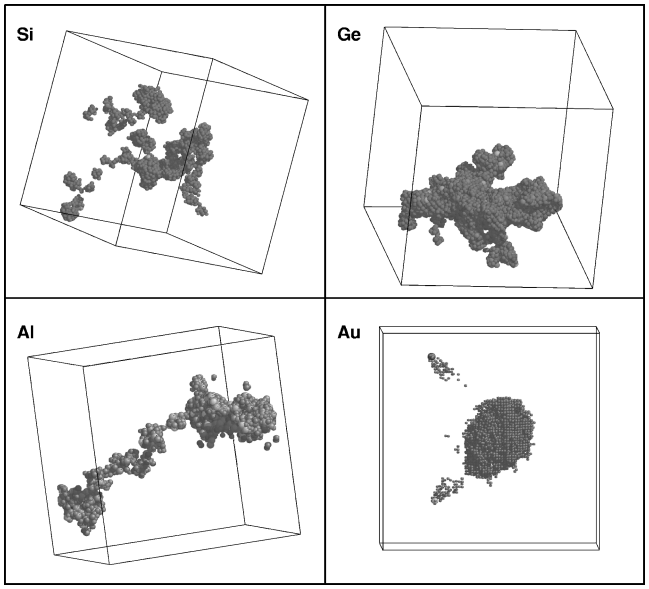

FIG. 2. Liquid atoms in 10 keV cascades in silicon (upper left), germanium (upper right), aluminum (lower left), and gold (lower right) (Ref. 61). The snapshots were chosen at times when the number of atoms in large continuous liquid regions was at a maximum. The atom size illustrates the kinetic energy of each atom, with the hottest atoms being larger. The bounding boxes show the total size of the simulation cells, which have been rotated to provide a clear view of the nature of the damage. In the gold cascade shown here, two replacement collision sequences emanate out from the center of the cascade, producing a trail of hot atoms in their wake.

and may migrate away from each other,[62,64] suggesting that they should be interpreted as separate defects. This makes 2 $a_0 \approx 10.8$ Å a natural upper limit for labeling two defects part of the same cluster. Unless otherwise mentioned, we thus use $r_{\mathrm{cl}} = 1.5 a_0 \approx 8.1$ Å in our analysis below. Analy-

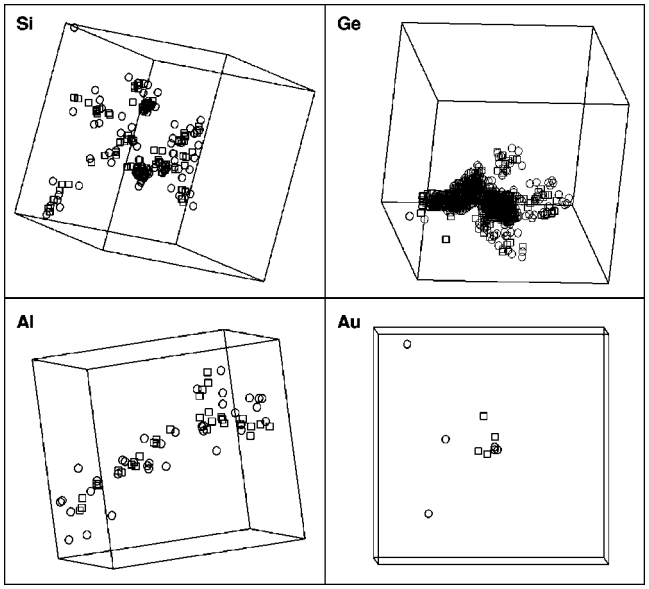

FIG. 3. Final defects created in 10 keV cascades in Si, Ge, Al, and Au. The cascades shown and the rotation of the cells are the same as in Fig. 2. Squares show the locations of vacancies and circles interstitials. The amorphous zones in Si and Ge appear as agglomerations of vacancies and interstitial in the figures.

TABLE IV. Fraction of isolated and clustered Wigner-Seitz defects in Si and Ge cascades. Note that the results depend somewhat on the choice of the value of r_{cl} (see discussion in text). N_{def} is the total number of defects in each case. F^{isol} gives the fraction of isolated defects, F_i^{isol} the fraction of isolated interstitials, and F_v^{isol} the fraction of isolated vacancies compared to the total number of defects. F^{clus}, F_i^{clus}, and F_v^{clus} give the fraction of defects, interstitials, and vacancies, respectively, in clusters with at least 6 defects. All fractions are given as percents of the total number of defects; since clusters with a size of 2–5 defects are not included, the total does not equal 100%. The error bars are the statistical error of the average.

Energy (keV)	N_{def}	F^{isol} (%)	F_i^{isol} (%)	F_v^{isol} (%)	F^{clus} (%)	F_i^{clus} (%)	F_v^{clus} (%)
Si 0.4	9±1	27±3	19±1	8±2	42±6	15±2	27±4
2	35±2	21±1	15±1	6.0±0.4	49±3	19±2	30±2
5	90±3	19±1	14±1	4.8±0.3	64±4	28±2	36±2
5[a]	169±4	11±1	10±1	0.8±0.1	81±2	35±1	46±1
10	196±5	13±1	11±1	2.7±0.2	68±2	32±1	36±1
Ge 0.4	10±1	23±4	21±3	2±1	42±12	23±7	21±6
2	103±3	6.4±0.5	5.6±0.4	0.8±0.2	91±3	43±2	48±2
5	286±11	2.5±0.2	2.4±0.2	0.1±0.1	95±4	46±2	49±2
5[b]	54±1	24±2	19±1	5.5±0.8	42±4	14±2	28±3
10	687±46	1.9±0.2	1.6±0.2	0.3±0.1	96±7	47±3	49±3

[a]Tersoff potential (Ref. 36).

[b]Unmodified Ge potential (see text).

ses using r_{cl} values of a_0 and $2a_0$ gave the same qualitative conclusions.

Table IV gives results for the distribution of defects into point defects and large clusters, and also values for how interstitials and vacancies are distributed among both groups. The table shows that the *fraction* of point defects decreases, and the fraction of large clusters increases with increasing cascade energy, in good agreement with the B and As cascade results of Caturla *et al.*[13] We also see that the relative amount of damage in clusters is about the same in the 5 keV and 10 keV cascades, a consequence of subcascade formation at these energies.

It is interesting to note that most of the isolated point defects are interstitials, both for the Tersoff and Stillinger-Weber interatomic potentials. These interstitials, which comprise 10–15 % of all defects, can either be formed by replacement collision sequences or by low-energy recoils. We have recently shown that due to the open crystal structure of Si, low-energy secondary or tertiary recoils having energies slightly above the threshold displacement energy have a large effect on cascade development in Si.[65] The above-mentioned fact that the Tersoff and Stillinger-Weber potentials give about the same number of point defects also indicates that the formation of these defects is a predominantly ballistic phenomenon.

To find out whether the interstitials were produced by replacement collision sequences or ballistic recoils, we evaluated the distance the extra atom in isolated interstitials had moved for the 10 keV cascades. About 85% of the interstitial atoms had moved farther than the nearest-neighbor distance from their initial site. Most of the atoms producing interstitials had moved 4–7 Å, the average being about 5 Å (not counting initial recoils which of course have moved very far). The distance from the interstitial to the closest vacancy was on average 14 Å, much more than the distance the atoms have moved. Since the isolated interstitials are located far from both vacancies and other interstitials, the recoils producing the interstitial must have been produced by previous recoils displacing atoms from perfect lattice sites and remaining there. Thus, the mechanism has some similarity to the well-known replacement collision sequences along $\langle 110 \rangle$ atom rows in fcc metals, even though it does not occur along a single well-defined lattice direction.

Since most of the isolated point defects are interstitials, it is clear that damage clusters will be deficient of atoms, visible as an excess of vacancies in the Wigner-Seitz analysis. One 10 keV event, for instance, produces about 7 large damage clusters on average (defined here as clusters having at least 6 defects) which jointly contain about 60 interstitials and 70 vacancies; i.e., they are deficient of 10 atoms. The same clusters can be expected to have roughly 600 disordered atoms (cf. Table III), and so the ''lack of atoms'' is about 1.7% of the total number of atoms. This lack of atoms can be expected to result in a -1.7% relaxation volume change in the amorphouslike phase that forms at the cluster.

The density of amorphous Si has been subject to a long-standing controversy, but the most recent experiments seem to indicate that the value is about 1.8% less than that of c-Si.[66] If we assume that (despite the enormously rapid quench rate in cascades) the amorphous phases produced during irradiation have the same density change as macroscopic a-Si, and take into account our estimate of a volume change of -1.7% due to the deficiency of atoms, we find that the volume change due to amorphous clusters produced by self-recoils in Si should be very close to zero, indicating that they may be hard to see using lattice parameter measurements or diffuse x-ray scattering.[67,68]

Considering that the other damage (the point defects and small clusters) has an excess of atoms, and cannot be considered amorphous, it is very likely that this damage will have a positive relaxation volume. If our argument for why amorphous clusters should have a negligible relaxation vol-

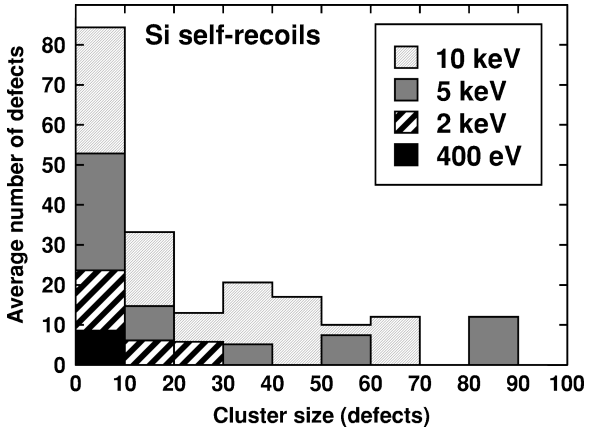

FIG. 4. Distribution of Wigner-Seitz defects as a function of the cluster size, measured as the number of defects each cluster contains. The data for each energy are overlayed on those of the higher energies. The numbers are the average over 6–10 events for each energy. Note that because of the limited number of events and clusters produced by them, the upper ends of the 5 keV and 10 keV distributions are not statistically significant. For instance, the value for 80–90 defects resulted from a single 5 keV event.

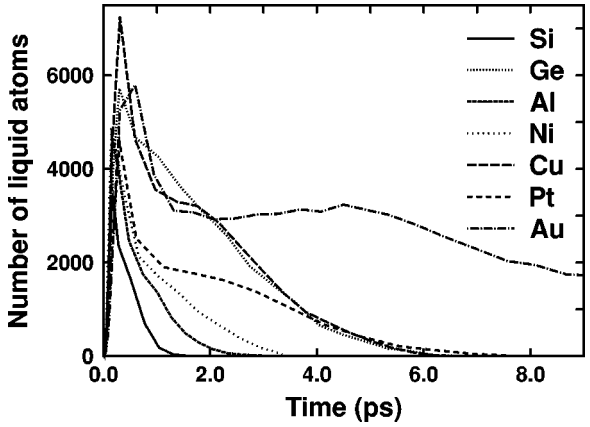

FIG. 5. Number of hot and liquid atoms as a function of time in representative 10 keV cascades in the seven different elements.

ume holds, the small-scale damage should result in a positive overall relaxation volume for ion-irradiated Si and, thus, a positive lattice parameter change. This agrees qualitatively with experimental observations of a positive lattice parameter change in Si during high-dose irradiation.[67,69,70]

Figure 4 shows a histogram of the distribution of defects with cluster size for the Si cascades. As already seen in Table IV, the number of defects in large clusters increases with energy. Note that the statistics for large 5 and 10 keV clusters is poor; the largest cluster was in fact (by coincidence) produced by a 5 keV cascade. Still, even for the 10 keV events the majority of damage is in fairly small clusters or point defects.

To summarize, our Si results show that classical potentials give a reliable picture of the cascade mixing, spatial distribution of damage, and production of isolated point defects. The isolated defects are predominantly interstitials. The clusters usually are amorphouslike regions, which—analyzed using space-filling Wigner-Seitz cells—contain many interstitials and vacancies, but a net balance of vacancies.

B. Germanium

Figures 2 and 3 show that the cascades in Ge have higher energy densities than in Si, and the resulting damage is well localized. The liquid region increases strongly in size with energy; for 400 eV cascades there typically is no real liquid, only hot atoms at the beginning of the simulation. At keV energies, a true liquid forms and exists for about 5 ps (cf. Fig. 5). The regeneration rate of covalently bonded tetrahedral lattices is low,[9] and so the liquid zones will form large damaged regions when the cascade cools down. Since the amount of damage is dependent on the size of the liquid region, the lower melting point of germanium compared to silicon explains why the amount of damage in germanium is considerably higher than in Si. For the same reason the modified Ge potential (with the correct, lower melting point) results in a much larger amount of damage than the unmodified one, which has only small amorphouslike damage pockets (see Table IV). The large difference in the damage numbers in the cascades simulated with the two versions of the potentials illustrates how the melting point strongly affects initial damage production in semiconductors.

The cluster analysis of germanium defects, using $r_{\mathrm{cl}} = 1.5a_0 \approx 8.1$ Å, showed that for the keV cascades almost all the damage is located in the large amorphous zones (cf. Table IV). Both the fraction and absolute number of isolated defects are smaller than that in Si. The number of isolated vacancies is vanishingly small, less than 1% of the total amount of damage. Most of the isolated defects are again interstitials. This conclusion holds for both versions of the Ge potentials. The large volume of the molten liquid and subsequent amorphous pockets result in almost all of the damage being contained within it, with only a few energetic recoils being able to ''escape'' the molten region.

IV. METALS AND COMPARISON

Damage production in metals has been studied to some extent.[8,17,19,22,23,57,71] It has become clear from past studies that at least in metals with atomic numbers $\sim$ 22 or more, cascade development is dominated by local melting in the core of the cascade.[9,22] Interstitials can be produced by replacement collision sequences[60] and are further separated from vacancies when the liquid core of the cascade collapses and drags vacancies to the center of the cascade.[9] Questions still to be answered are what happens to light metals like Al, and what effect the melting temperature and other material properties play on the cascades. Furthermore, although a loop-punching model for interstitial cluster formation has been suggested,[23] it appears that this cannot be the only possible mechanism of cluster formation.[72]

To probe these questions, we compare the nature of the heat spike, the ion beam mixing, and the final damage in all the different materials in this section. We also examine the mechanisms by which large interstitial clusters were formed in the heavy metals.

A. Heat spike development

We followed the time evolution of heat spikes using animations of the atom positions and the positions of hot and

liquid atoms during the simulation.[61] For the keV cascades, there were dramatic differences in the nature of the heat spikes in the different materials. The results for four of the materials are illustrated in Fig. 2.

In the heavy metals nickel, copper, platinum, and gold, which are dense close-packed materials (see Table I), the heat spikes were in all cases well localized and almost spherical, although in some cases parts of the liquid may become isolated during the cascade development (cf. Sc. IV C). The cascades form a large molten region which slowly cools down and recrystallizes. In a few of the events, like the one in gold shown in the figure, replacement collision sequences emanate out from the cascade and produce interstitials far from the cascade center. A metal with a higher melting point has a smaller number of liquid atoms, but the well-localized nature of the damage region is not affected by the melting point.

In the lighter and less dense aluminum, the initial recoil travels farther, and so the resulting molten regions are smaller and less well localized. At 10 keV, the cascade is divided into subcascades. Animation of other Al cascades shows that the subcascade formation begins between 2 and 5 keV, whereas in Si this threshold was about 1 keV. Since most other material characteristics in Si and Al are the same, this must be due to the difference in crystal structure, atomic density, and melting points. Although the 20% smaller atomic density of Si contributes into the difference, it is not likely this can account for all of it. We have recently shown that quite low-energetic ($\sim$100 eV) recoils can traverse farther in Si and Al due to the nature of the tetrahedral bonding, which will contribute into making the cascade even less dense.[65]

The cascades in germanium are not as spread out as those in Si due to the shorter range of Ge recoils. The threshold for subcascade formation is at or below 5 keV; the cascades clearly differ in shape from the almost spherical liquids formed in 10 keV Cu and Ni cascades (which are close in mass and atomic number to Ge). Simulations of 25–100 keV cascades in Ni (Ref. 73) showed that the energy threshold for subcascade formation in Ni is at or above 50 keV, at least an order of magnitude higher than in Ge. The much smaller atomic density in Ge than in Cu or Ni of course contributes to this effect. Since the mean ranges of ions in the materials differ by about a factor of 2 (cf. Table II), the difference in atomic density can be estimated to contribute by a factor of at most 8 into the subcascade formation threshold. The high melting point in Ni can be expected to lower the threshold energy, and so it cannot explain the remaining Ni-Ge difference. Thus it appears, as in Si and Al, that the difference in crystal structure also affects cascade development in heavier materials.

Figure 5 shows the time evolution of the number of hot and liquid atoms in representative 10 keV cascades in all the materials. The initial number of hot atoms is roughly proportional to the melting point, while the cooling down rate of the cascade depends on the atom mass, as can be expected. The hot atoms in the light elements Al and Si vanish in 1–2 ps, while the ones in Cu, Ge, Au, and Pt exist for about 6 ps or more, forming a clearly liquidlike region. From the figure it appears that the cooling *rates* of elements with the same mass are similar. But because of the difference in the initial number of molten atoms, the liquid in Al, Cu, and Au exists clearly longer than that in Si, Ni, and Pt, respectively.

B. Mixing

The cascade mixing results in Si and Al have been analyzed in detail elsewhere,[65] whence we only briefly summarize these results here. Comparison of the values for the mixing Q and number of displaced atoms N_{displ} in Table II shows that even though the number of displaced atoms is higher in Al and Cu than in Si and Ge, respectively, the mixing is much lower in Al and Cu than in Si and Ge. This result, which may at first seem self-contradictory, is explained by the different crystal structure. We have recently shown that the larger mixing in Si compared to Al is due to medium-energy secondary or tertiary recoils with energies of the order of $\sim$ 100 eV.[65] In Si these recoils can on average travel significantly farther than those in the close-packed Al structure, despite the similar atomic densities and atom numbers of Al and Si, resulting in a large increase in the mixing (which is proportional to the square of the atom displacement distance).

On the other hand, the much lower melting point of Al compared to that in Si will cause the molten regions produced in Al cascades to be larger than those in Si. The atoms in these regions are most likely recrystallized to a new lattice site when the cascade cools down, explaining why Al has much larger numbers of displaced atoms than Si. Since the molten regions recrystallize in a few ps, the atoms are not likely to travel far in the molten regions, making their contribution to the mixing significantly smaller than the contribution by the medium-energy recoils in Si. Thus the mixing in Si is almost entirely a consequence of the ballistic phase of the cascade.

The above argument also explains the results in Cu and Ge. Since the melting points are the same ($\sim$ 1250 K), the size of the molten regions and thus the number of displaced atoms are roughly the same. But Ge exhibits much larger values for the mixing coefficient because of the open nature of the bonding. Of all the light- and medium-heavy crystalline materials treated here Ge has the highest mixing (both experimentally[6] and in our simulations), which is due to the combined mixing-enhancing effects of a low melting point and an open crystal structure.

The mixing in gold and copper, which have relatively low melting points, is much larger than the mixing in nickel and platinum. Furthermore, the mixing in platinum simulated with the correct melting point is a factor of 3 smaller than the mixing in Pt simulated with the 30% too low melting point. The relative difference in the mixing is larger than the difference in the number of displaced atoms. All these effects are a consequence of the smaller volume and shorter time of existence of a liquid region in a material with a higher melting point; the smaller liquid volume reduces the number of displaced atoms, while the shorter lifetime of the liquid reduces the distance atoms can traverse while in it. In the case of Pt, the too low threshold displacement energy of the unmodified potential also contributed to the large difference in mixing.

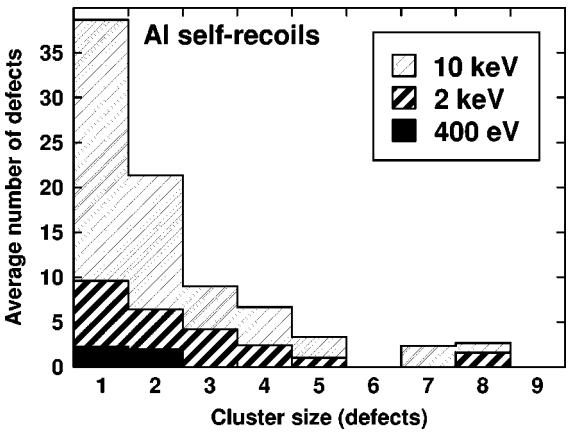

FIG. 6. Distribution of Wigner-Seitz defects as a function of the cluster size in Al, measured as the number of defects each cluster contains. The data for each energy are overlayed on those of the higher energies. The numbers are the average over 6–10 events for each energy. Because of the limited number of events and clusters produced by them, the upper ends of the 2 keV and 10 keV distributions are not statistically significant. Note that the abscissa scale is one order of magnitude less than in the corresponding Si figure.

C. Final damage states

The amount of final damage, as measured by the number of Wigner-Seitz-cell defects, is clearly larger in the tetrahedral semiconductors than in the metals. We again attribute this primarily to the effect of the crystal structure. In a recent study of cascades in predamaged samples, we showed that the ability of an fcc lattice to regenerate is much greater than that of a diamond lattice with covalent directional bonding.[9] This conclusion is supported by the results in Table II.

1. Aluminum

The amount of damage produced in all fcc metals except Al is very low compared to that in the semiconductors. The fact that Al differs in this respect from the other metals is clearly a consequence of its low mass, which causes the cascade to break up into subcascades at low energies. At 400 eV, where breakdown in subcascades has not occurred, the damage production is very close to that in the heavier metals. In the other fcc metals, the amount of damage produced is of the same order of magnitude for a given energy, and is only weakly affected by the melting point and material strength. This is because all the interstitials in the almost spherical liquid anneal out, and the only ones remaining are those which were formed close to the edge of the liquid and remain outside it. Since the volumes and surface areas of the single liquid region are similar in the heavy materials, defect production will also be. In Al the liquid is broken down into several smaller liquid zones, which decreases the probability that an interstitial will be trapped in the liquid. The relative increase in surface area may also play a role in the increased defect production.

Figure 6 shows the distribution of defects with cluster size in Al. The cluster size analysis was performed in the same way as the analysis for Si, using $r_{\mathrm{cl}}=2a_0\approx 6.1$ Å. Note that the cluster size scale on the abscissa is one order of magnitude less than the scale in the same figure for Si, Fig. 4. This shows that although the Al cascades form clusters as well, these clusters are much smaller than the clusters in Si. Analysis of the clusters showed that they were in all cases either pure vacancy or pure interstitial clusters. The small size and simple nature of the clusters in Al compared to Si reflects the importance of the crystal regeneration effect in fcc metals.

As for Si, we tracked the movement of the extra atom in isolated interstitials in Al. About 70% of the atoms came from a nearest-neighbor site, showing that most interstitials in Al are produced by replacement collision sequences along the close-packed $\langle 110\rangle$ rows. This is in clear contrast to Si, where we saw that only 15% of the interstitial atoms came from nearest-neighbor sites. The distance from the isolated interstitials to the closest vacancy was on average 16 Å (recall that in Si the same distance was 14 Å). This comparison shows that despite the similar mass and atomic density of Si and Al, cascade development in Al is much like that in other fcc metals, again emphasizing the crucial role of the crystal structure. On the other hand, the fact that the final separation between the interstitials and vacancies is about the same shows that the final state of damage is somewhat similar in Si and Al despite the clearly different damage production mechanisms. If we further assume that the amorphous pockets in Si anneal out (as they do at least at high temperatures[13]), the similarity in the initial state of damage is even more pronounced. During prolonged irradiation, on the other hand, damage in semiconductors accumulates into amorphous pockets and finally amorphizes the sample, whereas in metals the defects collapse into dislocations, but the sample remains crystalline.

2. Heavier metals

In the simulations of Si and Ge with different potentials, we noted that the choice of the interatomic potential strongly affects the nature and amount of the damage produced. In Si, furthermore, the mixing and number of displaced atoms were not affected by the choice of the potential. The results for copper and platinum, each one simulated with two different EAM potentials, behave exactly the opposite way. Both Cu potentials give the same amount and spread of the final damage, but 10–60 % different values for the mixing and number of displaced atoms. Similarly, for Pt there is a large difference in mixing, but only a small difference in the final amount of damage (cf. Sec. IV B). While both Cu potentials give almost exactly the same values for most physical quantities (see Table I), we found that the Sabochick-Lam potential gives a too high value for the threshold displacement energy [25 eV vs the experimental and Foiles potential value of 18 eV (Ref. 74)]. It appears that the Sabochick-Lam potential is slightly too hard in the lowest repulsive-energy region around 1–10 eV, making it difficult for low-energetic recoils to relocate and thus causing the lower mixing values seen in Table II. Still, the fact that both potentials in either Cu or Pt give the same amount of final damage suggests that EAM potentials which reproduce well basic material properties such as the elastic moduli are reliable in predicting the nature of damage produced in collision cascades.

The hot zones in silicon and germanium tend to freeze in as amorphous damage pockets in the final lattice, whereas in fcc lattices the liquid region usually regenerates almost perfectly. The defects left in the fcc lattices are mostly intersti-

tials created close to the surface of the liquid pockets or vacancies left in the center of a previously liquid region.[9] An analysis of the clusters formed in the heavier metals showed that, as in Al, all the damage clusters consist of either only interstitials or only vacancies. We will explore the formation mechanism of large interstitial clusters further below. The strength of the regenerative effect was well evident in one of the 400 eV Au simulations; this event had no final damage in the lattice, even though the maximum number of hot atoms in the same event was about 100.

The distribution of final Wigner-Seitz point defects is illustrated in Fig. 3. The events chosen for the figure and the rotations of the cell are the same as in Fig. 2. Comparison of the two figures show that in Al, Si, and Ge the final damage distribution is located in the regions of the cell which were hot or liquid during the cascade. In fcc metals replacement collision sequences can produce interstitials atoms outside the liquid core of the cascade, as seen in the gold event. But replacement collision sequences typically have lengths of only a few lattice constants, and some interstitials appear to be produced without any visible RCS's; long events like the one shown in the figures are quite rare. In fact, from our simulations it is apparent that the main mechanism separating interstitials and vacancies in metals is not long replacement collision sequences, which were once thought to be the dominating separation mechanism. Rather, the main reason for efficient defect separation is that interstitials are created at the outskirts of the liquid zone, whereas vacancies are dragged into the center of the liquid when it contracts.

Even though damage is created in a quite different manner in the two kinds of materials, the damage distributions, as measured by the root-mean-square displacement of interstitials from their center $\langle dR_{\mathrm{int}} \rangle$, are roughly the same in Si and Al on the one hand and all heavier elements on the other. In silicon and aluminum, which are split into subcascades at high energies, damage gets created along the ion path. This spreads out the damage in a large cell region. Despite the shorter mean range of Pt and Au self-ions compared to Cu and Ni, all of these metals have about the same extension of the damage due to the fact that most of the damage gets created in or around the liquid core of the cascade.

It is curious to note that despite the major differences in the cascade development, the end results of the cascades in all the materials treated here have some similarities. Isolated point defects are predominantly interstitials far from the cascade core, and the damage in the cores is vacancy rich. But whereas in semiconductors the damage in the cores is highly disordered, in metals it tends to take the form of small vacancy clusters in otherwise perfect crystal.

For most materials, a high melting point is related to high values of the elastic moduli, i.e. a hardness of the material and stiffness of the bonds (compare the bulk moduli and melting points of otherwise similar materials in Table I). At first thought, a lower melting point could thus be expected to result in more damage. This is true in the tetrahedral semiconductors because most of the hot regions freeze into amorphous damage zones as the cascade cools down. For the fcc metals, this is not found. Even though Cu has a lower melting point and is clearly softer than Ni, the amount of damage produced in these materials is about the same. The same is true for the two Pt potentials; although there is a difference

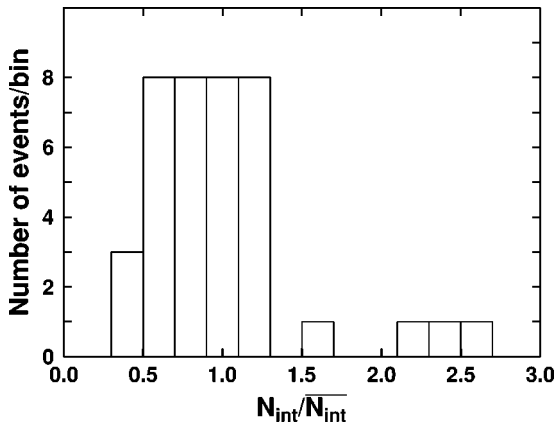

FIG. 7. Histogram of the number of events with a certain number of interstitials in the 10 keV events in the heavy metals Ni, Cu, Pt, and Au. To make the events comparable, the number of interstitials in each event has been divided by the average in the respective element. The three events with the largest damage production all produced large damage clusters.

of about 20–30 % in the amount of damage produced, it is much smaller than the difference of a factor of about 3 in the size of the liquid region. Again, this results from the strong tendency of fcc metals to regenerate into perfect lattice regions. Since all interstitials recombine with vacancies in the liquid zone, defect production is insensitive to T_{melt}. The difference in damage production between Au and Pt is most likely related to the difference in elastic strength between the two materials.

3. Interstitial cluster formation

The damage produced in the heavy metals was in most events in the form of isolated interstitials or vacancies, small clusters of 2–5 interstitials, or vacancy clusters in the center of the cell. An analysis of the nature of the clusters showed that (using $r_{\mathrm{cl}}=\frac{3}{2}a_0$) all of the defect clusters in all heavy metals were either pure interstitial clusters or pure vacancy clusters. Due to the close-packed lattice and the metallic bonding, formation of amorphouslike zones is highly unlikely in metals.

In 3 of the 39 10 keV events simulated in Ni, Cu, Pt, and Au with unmodified potentials a large interstitial cluster was formed. These clusters contained about 20–30 atoms ($\sim$ 10 Wigner-Seitz cells with more than 1 atom). In the same events, the total production of damage was clearly larger than in the average events. Figure 7 shows statistics of the number of Wigner-Seitz interstitials produced in all 39 events. To make events in the different materials comparable, the number of defects in each material has been divided by the average in that material. Even though the statistics is small, we see that the three ''cluster'' events clearly differ from the defect production distribution of the ''ordinary'' events. It is also curious to note that the total amount of damage in the ''cluster'' events falls in the same region, around 2.5 times the average, but with only three cluster-producing events we cannot state with certainty whether this is only a statistical aberration or due to some underlying physical principle.

The formation of similar interstitial clusters has been observed previously by Diaz de la Rubia and Guinan in a 25

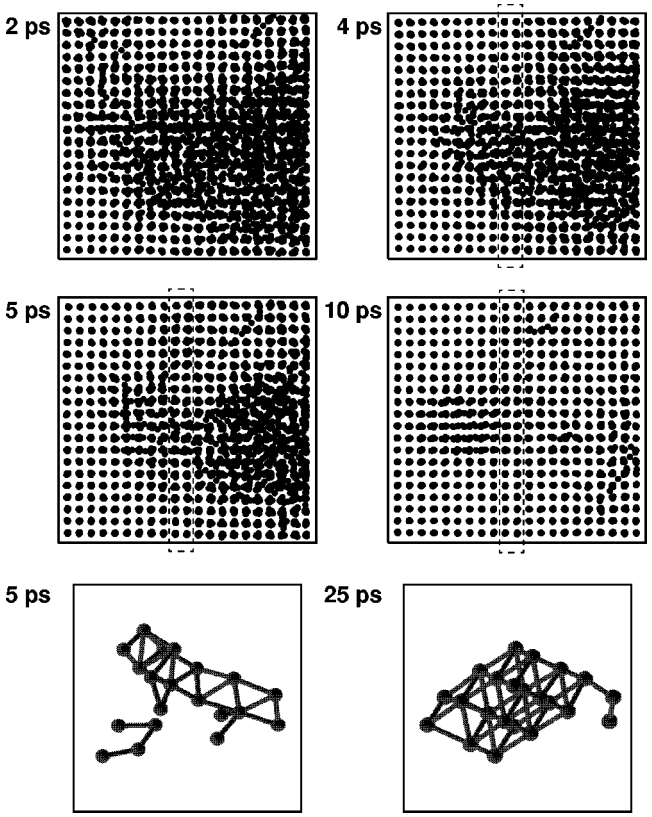

FIG. 8. Formation of a defect cluster in a 10 keV cascade in Pt. The top four figures show the atom positions in a $40\times40\times50$ Å^3 region of the simulation cell projected onto the *xy* plane. The two atom rows (highlighted with dashed rectangles) which crystallize and isolate part of the liquid are highlighted with a dashed contour. The lowest figures show the positions of atoms in the cluster at 5 and 25 ps.

keV cascade in copper.[23] They suggested that the cluster was formed by the punching of a dislocation loop by the high pressure present in the surface region of the liquid. The loop-punching mechanism requires the presence of very high pressures at the interface, and is recognizable from the coherent motion of the atoms forming the interstitial loop, although this was not clearly established in that work.[12]

The interstitial clusters we saw were not formed by the same mechanism. We followed the motion of the individual atoms which were part of the cluster, and found that they had moved largely randomly, as can be expected by atoms in the liquid zone of a cascade or on the edge of it. Furthermore, some atoms had moved 5–6 Å, while others moved only 1–2 Å; in the loop-punching mechanism, one would expect all atoms to move about the same distance in about the same direction. We did not see any such concerted motion of atoms in the clusters examined.

In one of the Pt events forming a cluster, the mechanism of cluster formation is clearly visible. The production of this cluster is illustrated in Fig. 8. The upper four figures show the positions of all atoms in a box around the cluster with a size of $40\times40\times50$ Å^3. The liquid formed by the collision cascade is visible as a disordered region in the figures, and extends far to the right from the region of the cell shown. At 2 ps, the liquid has a somewhat elongated form in one end, but is clearly part of the central liquid. Because of the high pressure and temperature in the center of the cell, this edge region of the liquid has an excess of atoms. At 4 ps, when the liquid has started to contract a crystallized ''neck'' is forming in the elongated part of the liquid; the location of the neck is shown with dashed lines in the figure. At 5 ps this neck has crystallized, isolating the extra atoms to the left of it, thus preventing them from collapsing back towards the center of the cell and recombining with vacancies there (as they otherwise would be likely to do). At 10 ps, we see that while the rest of the region has recrystallized to a mostly perfect crystal, an interstitial cluster has formed in the region with the isolated excess atoms.

The positions of atoms in the cluster are illustrated in the lower part of the figure. At 5 ps, the atoms are in a mostly disordered configuration. At 25 ps, they have collapsed into a more ordered state in three planes. Note that the rotation used in showing the atom positions is the same in both cases; it is thus evident that the shape of the cluster is completely different at 5 and 25 ps. Both the fact that the shape of the interstitial cluster is largely random and that the shape differ completely at 5 and 25 ps are contrary to what would be expected for a loop-punching mechanism.

We conclude that the ''liquid-isolation'' mechanism of cluster formation described above is a mechanism of damage formation in cascades not recognized previously. Although it has some similarity to the loop-punching mechanism, primarily that the damage gets formed close to the edge of the liquid zone of the cascade, it differs from loop punching in the sense that damage formation by liquid-isolation does not involve the concerted motion of atoms characteristic of loop-punching. We note, though, that it is possible that there are intermediate stages where some of the interstitial atoms are pushed outwards in concert with each other, while others end up there due to the thermal expansion of the liquid. If this is the case, the ''liquid-isolation'' and ''loop-punching'' mechanisms are opposite extreme ends of a damage formation process which can occur as a mixed state of the two as well.

Since the liquid-isolation mechanism of cluster formation clearly is more likely to occur the less spherical the liquid core of the cascade is, one can expect the number of clusters formed by it to increase with the initial recoil energy, as increasing recoil energies are likely to produce more elongated cascades and eventually subcascades. Indeed, in simulations of 50 keV cascades in Ni and Pd all cascades formed at least one large interstitial cluster. Details of these calculations will be published elsewhere.[73]

V. CONCLUSIONS

In this paper we have studied how different characteristics of materials affect damage production in collision cascades by comparing cascades in Si, Ge, Al, Ni, Cu, Pt, and Au.

We found that the crystal structure has a large effect on many damage production processes. The open nature of the diamond crystal structure and the slow regeneration of damage due to the covalent bonding enhance damage production and the mixing caused by cascades, while the close-packed fcc lattice exhibits a strong damage regeneration effect leading to much smaller amounts of final damage. Since the diamond structure does not lead to dense cascades, heat spikes

are not very important in the evolution of cascades in silicon.

The melting point has a large effect on damage production in semiconductors, but only a weak effect in metals due to the crystal regeneration effect. The strength of the material somewhat affects damage production, but clearly less than the crystal structure. Finally, the atomic mass and density of the sample element affect the spatial distribution of the damage and the energy at which cascades start to break up in subcascades.

A detailed study of damage production in Si showed that keV cascades produce damage predominantly in the form of isolated defects, most of which are interstitials, and amorphouslike damage clusters which on average have a little less atoms than perfect Si. The size of the damage clusters was found to depend strongly on the choice of the interatomic potential. In Al, by contrast, only small damage clusters are produced, and these are always either pure vacancy or pure interstitial clusters.

We identified a production mechanism of damage clusters in fcc metals by isolation of a liquid region with an excess of atoms from the center of a cascade core.

ACKNOWLEDGMENTS

The research was supported by the U.S. Department of Energy, Basic Energy Sciences under Grant No. DEFG02-91ER45439, and by the Academy of Finland. Grants of computer time from the National Energy Research Computer Center at Livermore, California, the National Center for Supercomputing Applications in Champaign, Illinois, and the Center for Scientific Computing in Espoo, Finland, are gratefully acknowledged.

[1] R. S. Averback and T. Diaz de la Rubia, in *Solid State Physics*, edited by H. Ehrenfest and F. Spaepen (Academic Press, New York, in press).

[2] J. Keinonen, A. Kuronen, P. Tikkanen, H. G. Börner, J. Jolie, S. Ulbig, E. G. Kessler, R. M. Nieminen, M. J. Puska, and A. P. Seitsonen, Phys. Rev. Lett. **67**, 3692 (1991).

[3] A. Kuronen, J. Phys. Condens. Matter **3**, 1363 (1991).

[4] *Sputtering by Particle Bombardment I*, edited by R. Behrisch (Springer, Berlin, 1981).

[5] J. R. Hahn, H. Kang, S. Song, and I. C. Jeon, Phys. Rev. B **53**, R1725 (1996), and references therein.

[6] See, e.g., B. M. Paine and R. S. Averback, Nucl. Instrum. Methods Phys. Res. B **7/8**, 666 (1985).

[7] J. F. Knudsen, P. M. Adams, D. L. Leung, R. C. Cole, and D. C. Mayer, Nucl. Instrum. Methods Phys. Res. B **59/60**, 1067 (1991).

[8] D. J. Bacon and T. Diaz de la Rubia, J. Nucl. Mater. **216**, 275 (1994).

[9] K. Nordlund and R. S. Averback, Phys. Rev. B **56**, 2421 (1997).

[10] P. J. Bedrossian, M.-J. Caturla, and T. Diaz de la Rubia, Appl. Phys. Lett. **70**, 176 (1997).

[11] R. S. Averback, J. Nucl. Mater. **216**, 49 (1994).

[12] T. Diaz de la Rubia, Nucl. Instrum. Methods Phys. Res. B **120**, 19 (1996).

[13] M.-J. Caturla, T. Diaz de la Rubia, L. A. Marques, and G. H. Gilmer, Phys. Rev. B **54**, 16 683 (1996).

[14] M. W. Finnis, P. Agnew, and A. J. E. Foreman, Phys. Rev. B **44**, 567 (1991).

[15] T. Diaz de la Rubia, A. Caro, M. Spaczer, G. A. Janaway, M. W. Guinan, and M. Victoria, Nucl. Instrum. Methods Phys. Res. B **80/81**, 86 (1993).

[16] A. J. E. Foreman, W. J. Phythian, and C. A. English, Radiat. Eff. Defects Solids **129**, 25 (1994).

[17] W. J. Phythian, R. E. Stoller, A. J. E. Foreman, A. F. Calder, and D. J. Bacon, J. Nucl. Mater. **223**, 245 (1995).

[18] H. Zhu, R. S. Averback, and M. Nastasi, Philos. Mag. A **71**, 735 (1995).

[19] F. Gao, D. J. Bacon, A. F. Calder, P. E. J. Flewitt, and T. A. Lewis, J. Nucl. Mater. **230**, 47 (1996).

[20] R. Smith, D. E. Harrison Jr., and B. J. Garrison, Phys. Rev. B **40**, 93 (1989).

[21] T. Diaz de la Rubia and G. H. Gilmer, Phys. Rev. Lett. **74**, 2507 (1995).

[22] T. Diaz de la Rubia, R. S. Averback, R. Benedek, and W. E. King, Phys. Rev. Lett. **59**, 1930 (1987).

[23] T. Diaz de la Rubia and M. W. Guinan, Phys. Rev. Lett. **66**, 2766 (1991).

[24] K. Nordlund, Comput. Mater. Sci. **3**, 448 (1995).

[25] M. P. Allen and D. J. Tildesley, *Computer Simulation of Liquids* (Oxford University Press, Oxford, England, 1989).

[26] J. R. Morris, C. Z. Wang, K. M. Ho, and C. T. Chan, Phys. Rev. B **49**, 3109 (1994).

[27] M. S. Daw, S. M. Foiles, and M. I. Baskes, Mater. Sci. Rep. **9**, 251 (1993).

[28] F. Ercolessi and J. B. Adams, Europhys. Lett. **26**, 583 (1994).

[29] S. M. Foiles, Phys. Rev. B **32**, 3409 (1985).

[30] M. J. Sabochick and N. Q. Lam, Phys. Rev. B **43**, 5243 (1991).

[31] H. Balamane, T. Halicioglu, and W. A. Tiller, Phys. Rev. B **46**, 2250 (1992).

[32] H. Feil, H. J. W. Zandvliet, M.-H. Tsai, J. D. Dow, and I. S. Tsong, Phys. Rev. Lett. **69**, 3076 (1992).

[33] F. H. Stillinger and T. A. Weber, Phys. Rev. B **31**, 5262 (1985).

[34] G. H. Gilmer, T. Diaz de la Rubia, D. M. Stock, and M. Jaraiz, Nucl. Instrum. Methods Phys. Res. B **102**, 247 (1995).

[35] J. Tersoff, Phys. Rev. B **37**, 6991 (1988).

[36] J. Tersoff, Phys. Rev. B **38**, 9902 (1988).

[37] K. Ding and H. C. Andersen, Phys. Rev. B **34**, 6987 (1986).

[38] Z. Q. Wang and D. Stroud, Phys. Rev. B **38**, 1384 (1988).

[39] H. H. Andersen and J. F. Ziegler, *The Stopping and Range of Ions in Matter* (Pergamon, New York, 1977), Vol. 3.

[40] K. Nordlund, N. Runeberg, and D. Sundholm, Nucl. Instrum. Methods Phys. Res. B **132**, 45 (1997).

[41] J. F. Ziegler, J. P. Biersack, and U. Littmark, *The Stopping and Range of Ions in Matter* (Pergamon, New York, 1985).

[42] K. Nordlund, J. Keinonen, and A. Kuronen, Phys. Scr. **T54**, 34 (1994).

[43] P. Lucasson, in *Fundamental Aspects of Radiation Damage in Metals*, edited by M. T. Robinson and F. N. Young, Jr. (ORNL, Springfield, 1975), p. 42.

[44] H. K. Mao, P. M. Bell, J. W. Shaner, and D. J. Steinberg, J. Appl. Phys. **49**, 3276 (1978).

[45] V. N. Antonov, V. Y. Milman, V. V. Nemoshkalenko, and A. V.

Zhalko-Titarenko, Z. Phys. B **79**, 233 (1990).
[46] J. Keinonen, K. Arstila, and P. Tikkanen, Appl. Phys. Lett. **60**, 228 (1992).
[47] J. F. Ziegler, computer code SRIM-96 (private communication).
[48] M. Ghaly, Ph.D. thesis, University of Illinois at Urbana-Champaign, 1995.
[49] K. Nordlund, M. Ghaly, and R. S. Averback, J. Appl. Phys. **83**, 1238 (1998).
[50] H. Hsieh, T. Diaz de la Rubia, R. S. Averback, and R. Benedek, Phys. Rev. B **40**, 9986 (1989)>
[51] A. F. Calder and D. J. Bacon, J. Nucl. Mater **207**, 22 (1993).
[52] Since the diamond crystal structure is not a Bravais lattice, the cells centered at the lattice atoms are strictly speaking Voronoy polyhedra. See, e.g., N. W. Ashcroft and N. D. Mermin, *Solid State Physics* (Saunders, Philadelphia, 1976), Chap. 4.
[53] M.-J. Caturla, T. Diaz de la Rubia, and G. H. Gilmer, in *Materials Synthesis and Processing Using Ion Beams*, edited by R. J. Culbertson, D. W. Holland, K. S. Jones, and K. Maex, MRS Symposia Proceedings No. 316 (Materials Research Society, Pittsburgh, 1994), p. 141.
[54] Subcascade breakdown is here used to mean a collision cascade in which the liquid formed by the cascade is broken down into spatially separated regions. Note that since in heavy materials the size of the melt can grow after the ballistic phase of the cascade, subcascade breakdown is not always a purely collisional phenomenon.
[55] M. O. Ruault, J. Chaumont, J. M. Penisson, and A. Bourret, Philos. Mag. A **50**, 667 (1984).
[56] D. M. Stock, G. H. Gilmer, M. Jaraz and T. Diaz d la Rubia, Nucl. Instrum. Methods Phys. Res. B **102**, 207 (1995).
[57] M. Ghaly and R. S. Averback, Phys. Rev. Lett. **72**, 364 (1994).
[58] M. Tang, L. Colombo, J. Zhu, and T. Diaz de la Rubia, Phys. Rev. B **55**, 14 279 (1997).
[59] H. Hensel and H. M. Urbassek, Phys. Rev. B (to be published).
[60] J. B. Gibson, A. N. Goland, M. Milgram, and G. H. Vineyard, Phys. Rev. **120**, 1229 (1960).
[61] A GIF animation of the time development of the collision cascades is available on the World Wide Web in http://beam.helsinki.fi/~knordlun/casc/.
[62] P. Ehrhart and H. Zillgen, in *Defects and Diffusion in Silicon Processing*, edited by T. Diaz de la Rubia and S. Coffa, MRS Symposia Proceedings No. 469 (Materials Research Society, Pittsburgh, in press).
[63] S. Uhlmann, T. Frauenheim, K. J. Boyd, D. Marton, and J. W. Rabalais, Radiat. Eff. Defects Solids **141**, 185 (1997).
[64] P. J. Partyka, K. Nordlund, R. S. Averback, I. K. Robinson, and P. Ehrhart, in *Diffuse X-ray scattering study of defects created by keV ion implants in Si*, edited by I. M. Robertson, G. S. Was, L. W. Hobbs, and T. Diaz de la Rubia, MRS Symposia Proceedings (Materials Research Society, Pittsburgh, 1997), p. 89.
[65] K. Nordlund and R. S. Averback, Appl. Phys. Lett. **70**, 3103 (1997).
[66] J. S. Custer, M. O. Thompson, D. C. Jacobson, J. M. Poate, S. Roorda, W. C. Sinke, and F. Spaepen, Appl. Phys. Lett. **64**, 436 (1994).
[67] W. Mayer, D. Grasse, and J. Peisl, Phys. Status Solidi A **87**, 583 (1985).
[68] K. Nordlund, P. Partyka, and R. S. Averback, in *Defects and Diffusion in Silicon Processing* (Ref. 62).
[69] A. R. Chelyadinskii, Sov. Phys. Solid State **18**, 506 (1976).
[70] J. Burgeat and R. Colella, J. Appl. Phys. **40**, (1969).
[71] V. G. Kapinos and D. J. Bacon, Phys. Rev. B **53**, 8287 (1996).
[72] T. Diaz de la Rubia, Nucl. Instrum. Methods Phys. Res. B **120**, 19 (1996).
[73] K. Nordlund and R. S. Averback (unpublished).
[74] K. Urban, B. Saile, N. Yoshida, and W. Zag, in *Point Defects and Defect Interactions in Metals*, edited by J.-I. Takamura (North-Holland, Amsterdam, 1982), p. 783.